Research Article

Khalid G. Biro Turk*, Mohammed A. Alsanad

Estimation of water consumption and productivity for wheat using remote sensing and SEBAL model: A case study from central clay plain Ecosystem in Sudan

https://doi.org/10.1515/opag-2022-0230
received July 3, 2023; accepted October 9, 2023

Abstract: Remote sensing (RS) can efficiently support the quantification of crop water requirements and water productivity (WP) for evaluating the performance of agricultural production systems and provides relevant feedback for management. This research aimed to estimate winter wheat water consumption and WP in the central clay plain of Sudan by integrating remotely sensed images, climate data, and biophysical modelling. The wheat crop was cultivated under a centre-pivot irrigation system during the winter season of 2014/2015. The Landsat-8 satellite data were used to retrieve the required spectral data. The Surface Energy Balance Algorithm for Land (SEBAL) was supported with RS and climate data for estimating the Actual Evapotranspiration (ETa) and the WP for the wheat crop. The SEBAL outputs were validated using the FAO Penman–Monteith method coupled with field measurements and observation. The results showed that the seasonal ETa ranged from 400 to 600 mm. However, the WP was between 1.2 and 1.5 kg/m^3 during the wheat cycle. The spatial ETa and WP maps produced by the SEBAL model and Landsat-8 images can improve water use efficiency at field scale environment and estimate the water balance over large agricultural areas.

Keywords: actual evapotranspiration, water productivity, landsat-8 images, SEBAL model, water use efficiency

*** Corresponding author: Khalid G. Biro Turk,** Water Studies Centre, King Faisal University, P. O. Box 400, Al-Ahsa 31982, Saudi Arabia; Faculty of Agricultural and Environmental Sciences, University of Gadarif, P. O. Box 449, Gadarif, Sudan, e-mail: kturk@kfu.edu.sa, khalidturk76@yahoo.co.uk
Mohammed A. Alsanad: Department of Environment and Agricultural Natural Resources, College of Agricultural and Food Sciences, King Faisal University, P.O. Box 420, Al-Ahsa 31982, Saudi Arabia

1 Introduction

The water used for crops is crucial, especially in arid and semi-arid regions [1]. Therefore, water use efficiency is the key input for irrigation scheduling, and it is required to increase available water resources, improve soil quality, and increase crop productivity [2]. Kijne et al. [3] reported that the amount of water required for food production in the world by 2050 would be around 4,500 km^3/year from the current, which is ~7,000 km^3/year. They estimate that water productivity (WP) improvements could save up to 2,200 km^3/year reducing the future additional needs to ~2,300 km^3/year. Therefore, there is a need to widen the perspectives on water management from the farm level to the watershed level and integrate land-use-related water demands in resource negotiations and priority settings.

The WP (kg/m^3) is defined as the ratio between crop production (kg/ha) and the water consumption (m^3) per unit area (ha) [4,5]. Therefore, precise estimation of crop yield and crop water requirements (i.e. crop actual evapotranspiration) is essential for computing WP [6,7]. Accordingly, careful estimation of crop water productivity (CWP) becomes necessary for proper water management and improving decision-making processes for irrigation water use [8].

Remote Sensing (RS) and the Geographic Information System (GIS) are vital techniques for assessing the irrigation performance and spatial distribution of water use and WP [8]. RS and GIS can explore irrigation systems and CWP from field level to large-scale agricultural areas [8,9].

The Surface Energy Balance Algorithm for Land (SEBAL) model showed significant development over the last decade, which increased its ability to estimate ET using a wide range of satellite data. SEBAL model has been successfully applied in many studies for determining the crop water requirement. The estimation of water consumption and productivity for rice was performed using the SEBAL model in the Songnen

Plain of China [10]. However, the application of the SEBAL model to estimate the Actual Evapotranspiration (ETa) for cotton crops in the Mato Grosso State of Brazil assists in the management of the irrigation schedule in irrigated cropping systems [11]. In Pakistan's Indus Basin Irrigation System, the SEBAL model was used to improve the strategic planning and management of available water resources in the basin [12]. However, the SEBAL model was evaluated to quantify the water required by the winter wheat in many countries. In North China, the application SEBAL for ET estimation resulted in an error of 4.3% throughout the entire growing stages of the winter wheat [13]. Moreover, the potential of SEBAL for improving on-farm water management for wheat was investigated in Pakistan [14]. The ET seasonal trend for wheat was estimated in Lebanon's Bekaa valley with a mean value of 620 mm [15].

Wheat (*Triticum aestivum*) is one of the most important cereal crops cultivated widely in many parts of the world. For more than three decades, wheat production has become an issue in Sudan because it affects the food security and diet of the population. The total cultivated area by wheat in Sudan increased from 16,400 ha in 1961 to 400,000 ha in 2009. In contrast, the maximum harvested area was in 1991 from 462,928 ha [16]. Consequently, wheat yield increased from 25 to 900 tons between 1961 and 2020 [17]. The variations in wheat production and cultivated area can be attributed to Sudan's many challenges. These challenges include climate change, population growth, food prices, financial disruptions, and political fluctuations. Therefore, producing more food in large-scale agricultural schemes requires the re-shaping of agricultural water use in these major food-growing areas [18].

The increasing competition over the water resources in the Nile Basin requires a better understanding of water uses and management related to water consumption [19]. Accordingly, improving the ability of decision-makers, investors, and farmers to make informed decisions about water resources management in Sudan and the costs of CWP is crucial.

This article aimed to estimate wheat water consumption and WP in the central clay plain of Sudan by integrating RS data, climate data, and the SEBAL model. Also, efforts were made to compare the outputs of the remotely sensed data and the actual water applied at the field based on the farm records.

2 Materials and methods

2.1 Study area

The study site (Alwaha farm) is located on the East bank of the Blue Nile within the central clay plain of the Sudan, which includes the Gezira scheme (Figure 1). It is located about 60 km southeast of Khartoum, the capital of Sudan. Alwaha farm covers an area of about 14,500 Hectare (ha). The main source of water is the Blue Nile through pumps. Sprinkler irrigation through the centre pivot system is the main water supply method on the farm. The main crops produced by the farm are Alfalfa, Wheat, Corn, and Rhodes grass.

The climate of the study site is characterised by a hot, dry summer season from April to June/July, a rainy season from August to September/October, and a winter season from November/December to March. The rainfall at the site is minimal, about 100–150 mm/year. The relative humidity ranges from 60% during the rainy season to about 30% in the dry months. Consequently, only sparse vegetation grows at the study site and when the rainy season is relatively wet. The soils of the study site were dominated by the sandy pediplains and basement or Nubian outcrops [20]. However, aggradation clay plains, as well as the riverine alluvial deposits, also exist in the area.

The crop calendar shows that the wheat crop was cultivated during the winter season of 2014/2015 (Table 1), with a total area of 1,150 ha covering 20 pivots. However, the area of each pivot varies from 24 to 61 ha for the total of twenty pivots planted by wheat.

2.2 Data sets used

2.2.1 Landsat-8 data

8 Landsat-8 satellite imageries were obtained from the United States Geological Survey (USGS) website (https://earthexplorer.usgs.gov/). The main characteristics of these data are shown in (Table 2). The Landsat-8 images were acquired with a cloud cover of less than 10%. The nearest neighbour method was used to geometrically and radiometrically correct all images and resampled them into a pixel size of 30 × 30 m.

2.2.2 Digital elevation model (DEM) data

A global DEM was generated from the Advanced Spaceborne Thermal Emission, and Reflection Radiometer (ASTER) was used for topographic correction [21]. The DEM is known as ASTER GDEM, and it is obtained from the USGS website. It is a 30 m grid size DEM produced by the National Aeronautics and Space Administration and the Ministry of Economy, Trade, and Industry of Japan.

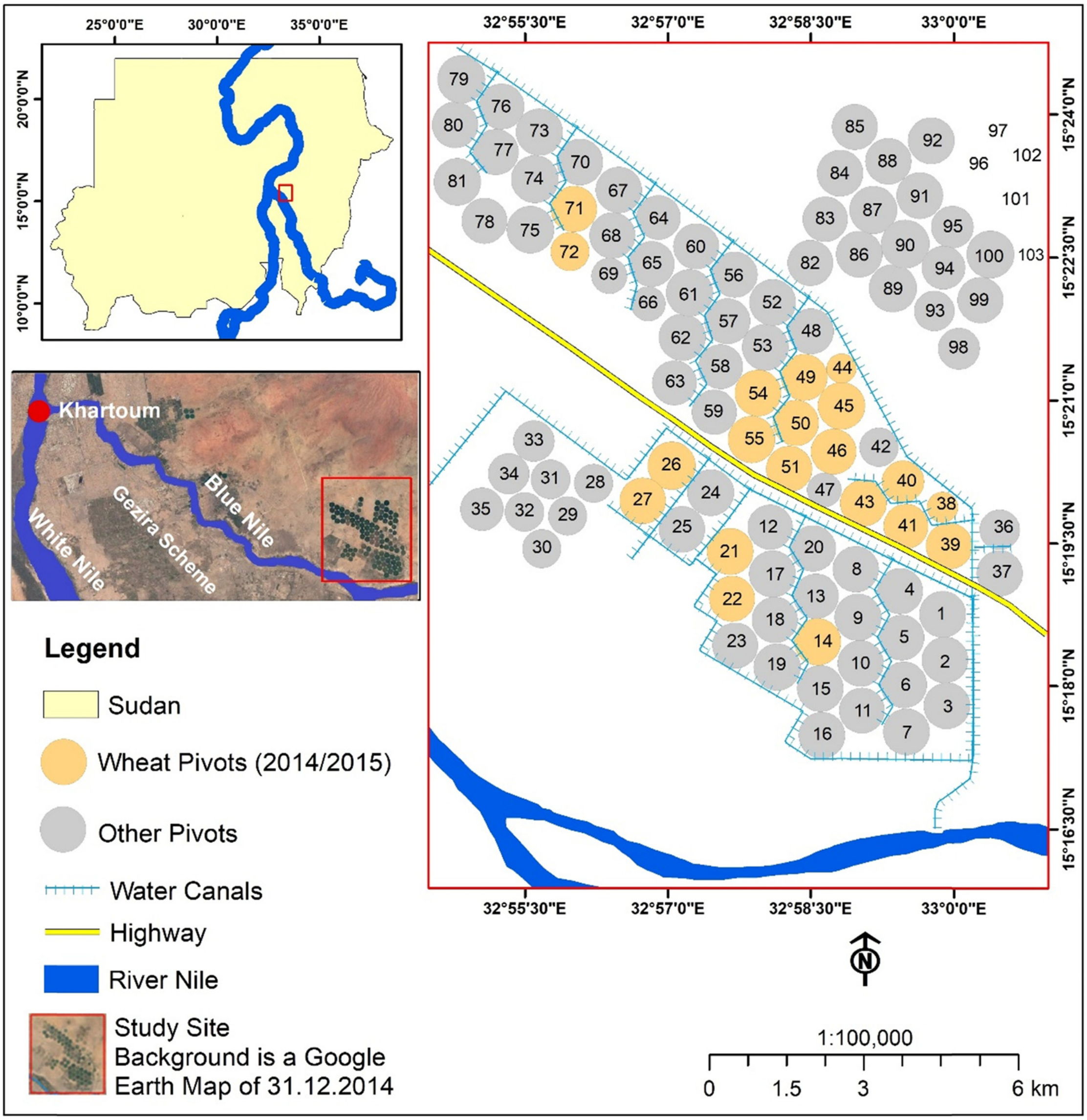

Figure 1: Location of the study area.

2.2.3 Meteorological data

Climatic data of the study site were obtained from the local metrological station located on the farm. These data include air temperature, net radiation, relative humidity, wind speed, vapour pressure, and precipitation (Figure 2). The collection of climate data was made on an hourly and daily basis. In addition, missing climatic data were filled in from the Global Land Data Assimilation System [23]. Figure 3 shows the correlations between the local metrological station and the GLDAS data used for filling the gap.

Table 1: Winter wheat crop calendar during 2014/2015

2014		2015		
Nov	**Dec**	**Jan**	**Feb**	**Mar**
Sowing		Growing		Harvesting

2.2.4 Field measurement data

The field data were collected from the daily records of the Alwaha farm. These records include the crop age, applied irrigation based on total operation pivot hours, and grain yield for each pivot.

Table 2: Landsat-8 satellite sensor specifications [22]

Sensor	Bands type	Wavelength (μm)	Spatial resolution (m)
Operational Land Imager	Band 1, Coastal aerosol	0.43–0.45	30
	Band 2, Blue	0.45–0.51	30
	Band 3, Green	0.53–0.59	30
	Band 4, Red	0.64–0.67	30
	Band 5, Near Infrared	0.85–0.88	30
	Band 6, Short-wave Infrared 1	1.57–1.65	30
	Band 6, Short-wave Infrared 2	2.11–2.29	30
	Band 8, Panchromatic	0.50–0.68	15
	Band 9, Cirrus	1.36–1.38	30
Thermal Infrared Sensor	Band 10, Thermal Infrared 1	10.60–11.19	100
	Band 10, Thermal Infrared 2	11.50–12.51	100

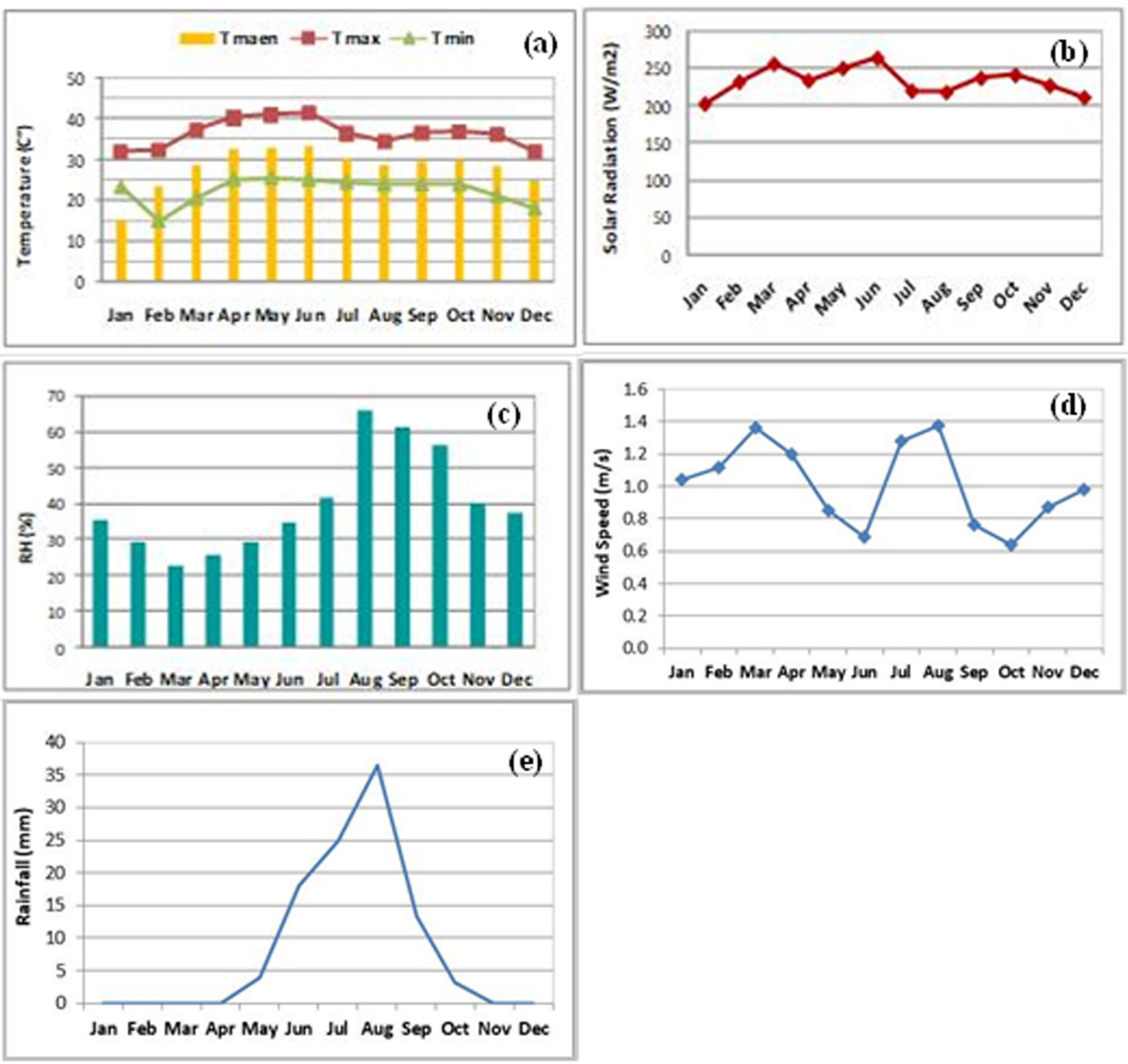

Figure 2: Climate data measured at Alwaha Farm meteorological station during 2014/2015: (a) temperature, (b) solar radiation, (c) relative humidity, (d) wind speed, and (e) rainfall.

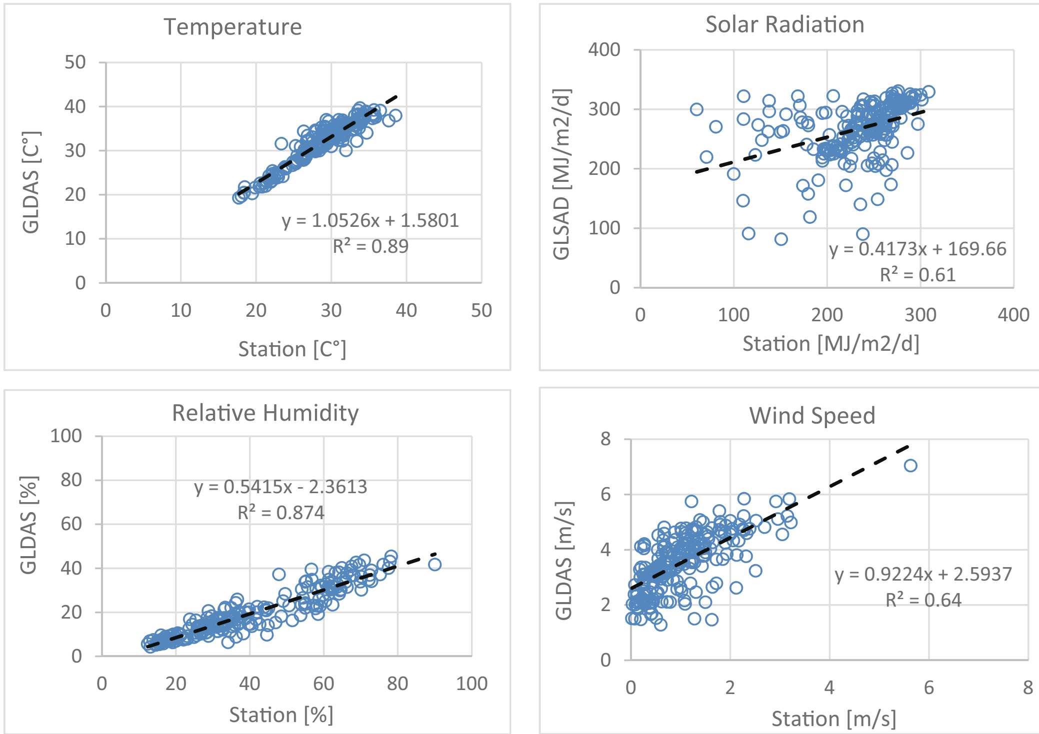

Figure 3: Comparison between the Climate Data at Alwaha farm meteorological station and the GLDAS data.

2.3 Methodology applied in this study

The methodology applied in this study includes data input, data processing, and the main outputs (Figure 4). ERDAS IMAGINE 9.2 software and the ArcGIS 10.2 software were used for data analysis and visualisation.

2.3.1 SEBAL model for ET calculation

The SEBAL model calculated the ETa from Landsat-8 satellite images [23]. The model key input data consist of satellite surface albedo measurements, leaf area index (LAI), NDVI, and surface temperature (T_s). In addition to the satellite data, the SEBAL model requires minimum inputs of routine weather data (Part 2.2.3).

The SEBAL algorithm computes the latent heat flux as the residue of the energy balance equation [24–26]:

$$\lambda \mathrm{ET} = R_n - G - H, \tag{1}$$

where R_n is the net radiation over the surface (W/m^2), G is the soil heat flux (W/m^2), H is the sensible heat flux (W/m^2), λET is the latent heat flux (W/m^2), and λ is the latent heat of vaporisation (J/kg).

The net radiation (R_n) was calculated using surface reflectance, and surface temperature (T_s) derived from satellite imagery as indicated by Allen et al. [27].

The soil heat flux (G) is the heat flux rate stored or released into the soil and vegetation due to conduction. The ratio G/R_n was computed as developed by Bastiaanssen et al. [28].

The sensible heat flux (H) is the heat loss rate to the air by convection and conduction due to a temperature difference. H was determined using the aerodynamic-based heat transfer equation as described by Mohajane et al. [29].

The instantaneous value of ET in equivalent evaporation depth was computed as:

$$\mathrm{ET_{inst}} = 3{,}600 \frac{\lambda \mathrm{ET}}{\lambda}, \tag{2}$$

where $\mathrm{ET_{inst}}$ is the instantaneous ET (mm/h), 3,600 is the conversion from seconds to hours, λET is the latent heat flux (W/m) consumed by ET, ρw is the density of water (1,000 kg/m^3), and λ is the latent heat of vaporisation (J/kg) and was computed as follows [30]:

$$\lambda = [2.501 - 0.00236(T_s - 273.15) \times 10^6]. \tag{3}$$

The reference ET fraction ($\mathrm{ET_0}F$) or crop coefficient (kc) was calculated based on $\mathrm{ET_{inst}}$ for each pixel, and $\mathrm{ET_0}$ was obtained from local ground weather stations [30].

$$\mathrm{ET_0}F = \mathrm{ET_{inst}}/\mathrm{ET_0}. \tag{4}$$

The daily values of ET (ET24) (mm/day) for each pixel were calculated as follows:

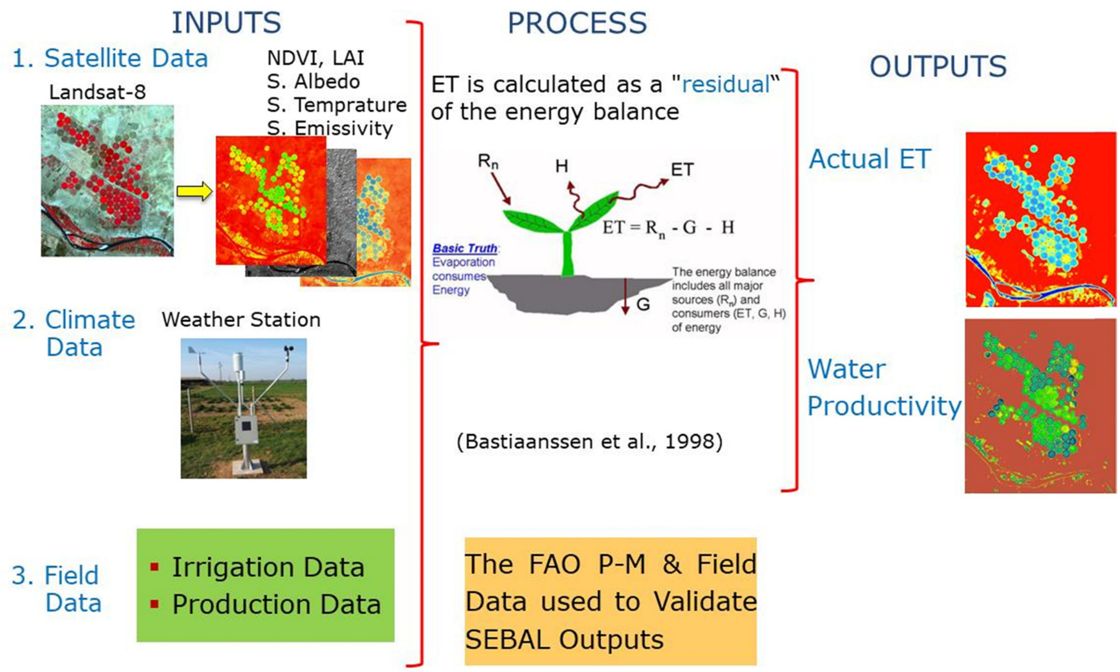

Figure 4: A flowchart explains the methodology process.

$$ET_a = ET_0F \times ET_024, \tag{5}$$

where ET_0F is the reference ET fraction, ET_024 is the cumulative alfalfa reference for the day (mm/day), and ET_a is the actual evapotranspiration for the entire 24-h period (mm/day).

The actual monthly and seasonal ET was calculated using daily ET data as follows [30]:

$$ET_{a,\text{period}} = \sum_{i=m}^{n} ET_0F \times ET_024, \tag{6}$$

$$ET_{a,\text{seasonal}} = \sum ET_{a,\text{period}}. \tag{7}$$

Allen et al. [31] showed that one cloud-free satellite image per month is sufficient to develop ET_0F curves for seasonal ET_a estimations.

2.3.2 CWP estimation

The CWP for each pivot was calculated using the yield data of winter wheat according to equation (8) [12]:

$$CWP = \frac{Y}{10 \times ET_{a,\text{seasonal}}}, \tag{8}$$

where CWP is the crop water productivity (kg/m^3), Y the wheat yield (kg/ha), and $ET_{a,\text{seasonal}}$ (mm) is the total ET_a throughout the growing season of the winter wheat.

2.4 SEBAL model validation and statistical analysis

The calculated ETa from Landsat-8 images and the SEBAL model was validated using the FAO P-M method [32]. This method was used to calculate the reference crop evaporation (ET_0) from the actual climate data in the study area as follows:

$$ET_0 = \frac{0.408\Delta(R_n - G) + \gamma\frac{900}{T+273}U2(\text{es} - \text{ea})}{\Delta + \gamma(1 + 0.34U2)}, \tag{9}$$

where ET_0 is the reference evapotranspiration (mm/day), Δ is the slope vapour pressure curve (kPa/°C), γ is the psychrometric constant (kPa/°C), T is the mean daily air temperature at 2 m height (°C), $U2$ is the wind speed at 2 m height (m/s), es is the saturation vapour pressure (kPa), ea is the actual vapour pressure (kPa), and (es – ea) represents the saturation vapour pressure deficit (kPa).

The crop coefficient (kc) for the winter wheat was determined based on the study by Allen et al. [32]. The ET_0 obtained from the FAO P-M method and the kc were used to calculate the ET_a depending on actual weather data as follows:

$$ET_a = ET_0 \times kc. \tag{10}$$

The ET_a resulting from the FAO P-M method was used to validate the ET_a obtained from the SEBAL model.

Statistical indices include the mean relative error (MRE), the root mean square error (RMSE), and the normalised root mean square error (NRMSE) were used to measure the differences between the predicted and observed daily ETa by the SEBAL, the FAO P-M method, and the applied irrigation on the farm. These indices are shown in the following equations [33]:

$$\mathrm{MRE} = \sum_{i=1}^{n} \left| \frac{\rho_i - O_i}{O_i} \right| \times 100\%, \tag{11}$$

$$\mathrm{RMSE} = \sqrt{\frac{\sum_{i=1}^{n}(O_i - P_i)^2}{n}}, \tag{12}$$

$$\mathrm{NRMSE} = \frac{\mathrm{RMSE}}{\bar{O}} \times 100\%, \tag{13}$$

where n is the number of samples; ρ_i and O_i are the predicted value and observed value, respectively; $\bar{O}$ is the mean value of the observed value.

Moreover, the coefficient of variation (CV) was used to measure the precision of the ETa predicted by the SEBAL model. The CV was computed as follows [33]:

$$\mathrm{CV} = \frac{\mathrm{SD}}{\bar{\rho}}, \tag{14}$$

where $\bar{\rho}$ and SD are the mean value and the standard deviation of the predicted value, respectively.

3 Results and discussions

3.1 Water consumption for wheat

The spatial distribution of the daily ETa estimated using the SEBAL model is shown in Figure 5. The daily ETa varied from 0 to 6 mm/day; pivots with exposed soil were those that did not present ETa. The average daily ETa in the wheat cycle for the twenty pivots ranged between 3.25 and 4.76 mm/day (Figure 6). In the early of the growing season, the daily water consumption of wheat can be less than 2 mm/day. However, the rates of water use increase for the winter wheat, reaching a level of 5–8 mm/day as the canopy enlarges during tillering and stem elongation [34].

The monthly ETa maps of wheat show variability of 0–200 mm/month (Figure 7). Vegetated pivots were those with the highest values and pivots with exposed soil that had the lowest values. The variation of monthly ETa within

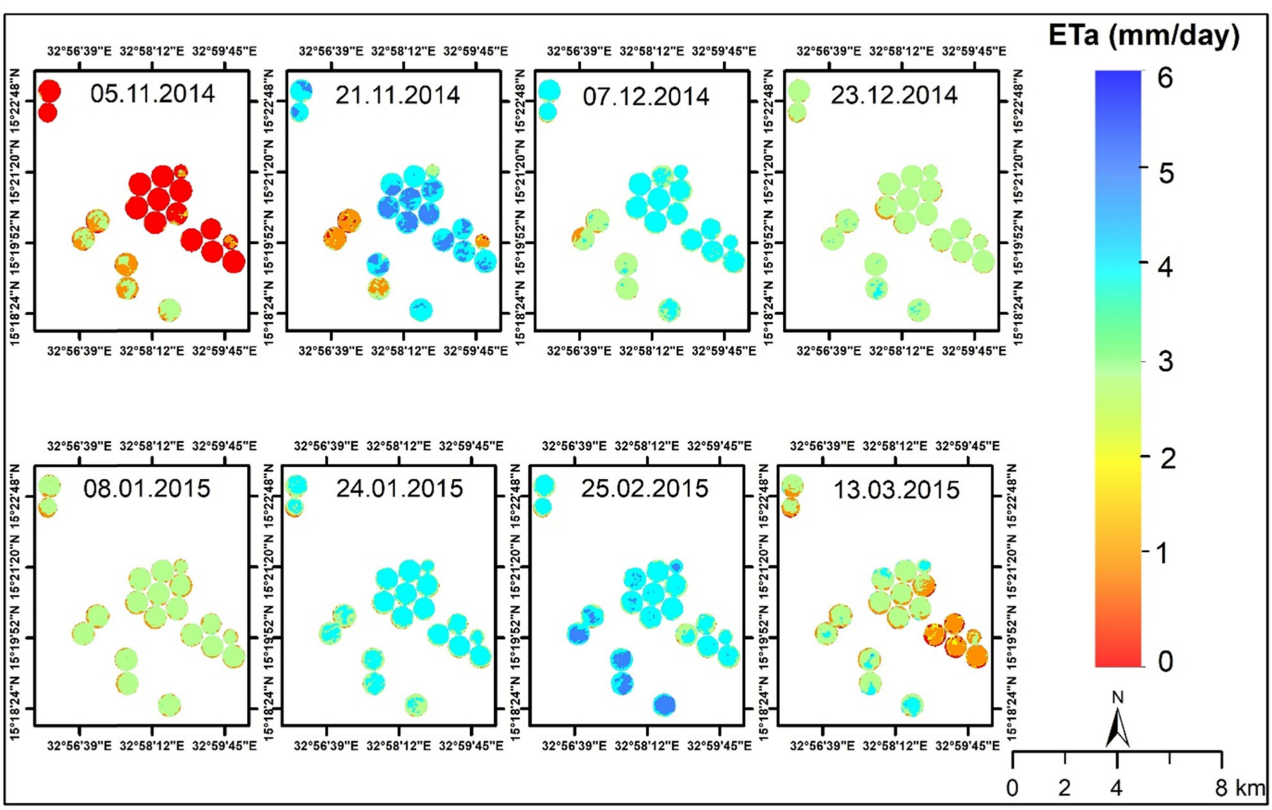

Figure 5: Spatial distribution of the daily ETa.

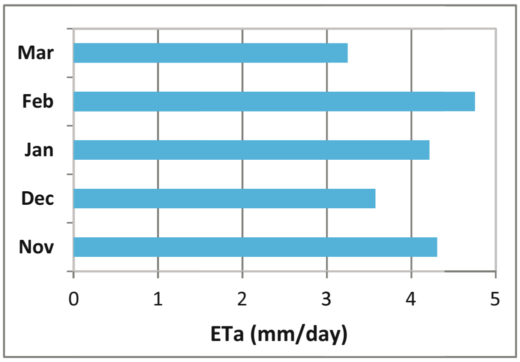

Figure 6: The mean daily ETa during the winter wheat growing season.

the pivots can be attributed mainly to the different cultivation dates of the winter wheat and the daily field operations applied along with the various pivots.

The accumulated seasonal ETa ($ET_{a,seasonal}$) during the phenological cycle of the wheat crop was in the range of 400–600 mm (Figure 7). The winter wheat cultivated in the Gezira Scheme located within the region of the study site showed an average seasonal ETa of 670 mm [35]. Nevertheless, the irrigation method in the Gezira Scheme is the surface furrow irrigation system. In the North China Plain, the average and maximum water consumption of winter wheat estimated by the SEBAL model were 424 and 475 mm, respectively [12].

3.2 CWP for wheat

The spatial distribution of the CWP is presented in Figure 8. The daily WP of winter wheat increased from the emergence phase, reached its maximum level in the anthesis phase, and then decreased during the maturity phase. The highest values of daily WP across the twenty pivots were observed during December (Figure 9). However, during the peak establishment and flowering stages in January and February, the daily WP ranged between 1.0 and 1.4 kg/m^3.

The seasonal WP ranged from 1.2 to 1.5 kg/m^3 (Figure 8). This WP was in the FAO [34] range of 1.2–1.2 kg/m^3. Moreover, the PW of winter wheat resulting from Alwaha Farm was compared with that produced at the Global Scale, the Nile Delta in Egypt, and the Gezira scheme in Sudan (Figure 10). The WP in Alwaha Farm was lower than the Global Scale by 43%. The differences in crop calendar, climate, agricultural inputs, and technologies increased the WP significantly on Global Scale compared to Alwaha

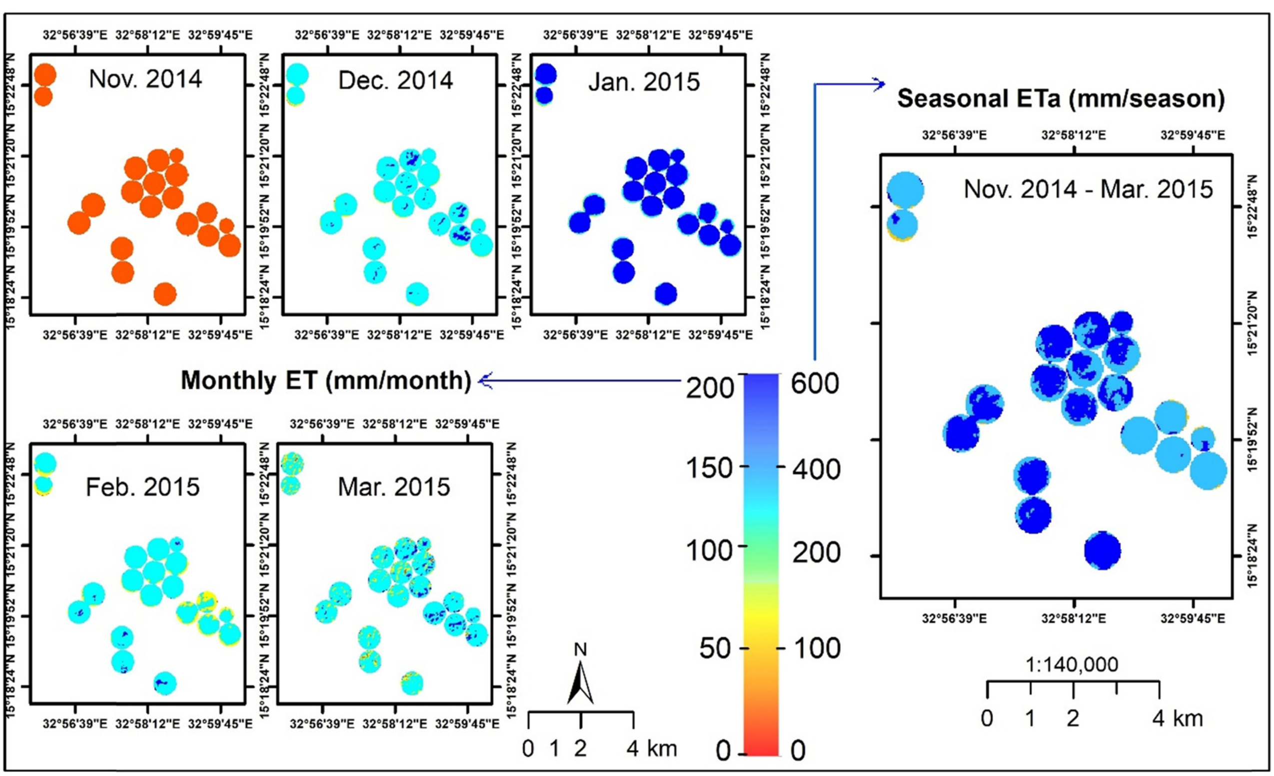

Figure 7: Spatial distribution of the monthly and seasonal ETa.

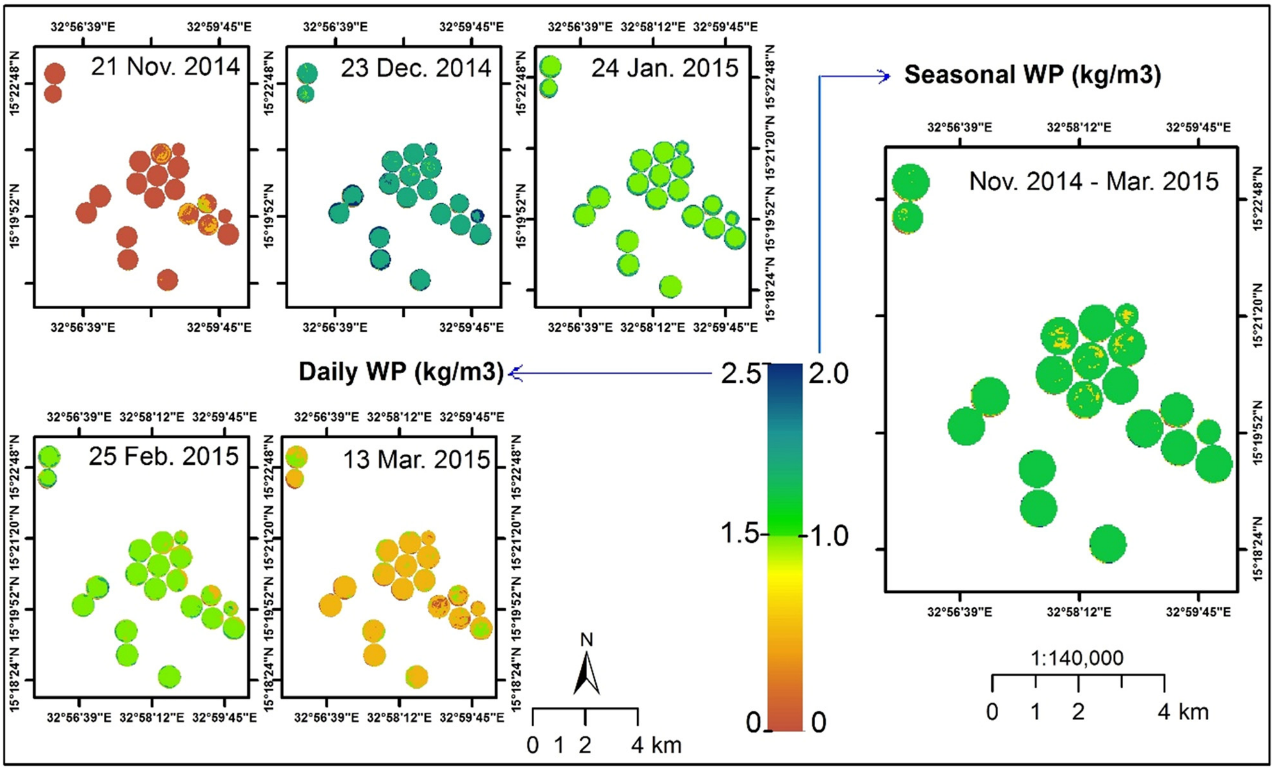

Figure 8: Spatial distribution of the daily and seasonal WP.

Farm. The change in WP between the Nile Delta and Alwaha Farm is less than 1% since the two systems apply the same level of agricultural inputs, such as fertilizers and pesticides [36]. The WP in Alwaha Farm is higher by 65% compared to the Gezira Scheme. The low irrigation efficiency in the Gezira Scheme was mainly attributed to the mismanagement of irrigation water at the field scale [37]. Furthermore, the level of investment in modern irrigation systems and agricultural inputs is considerable in Alwaha Farm compared to the wheat fields in the Gezira Scheme.

Raising WP at the field level can be achieved by selecting appropriate cultivars, planting methods, minimum tillage, timely irrigation, nutrient management, and improved drainage [38,39]. Moreover, introducing water-saving irrigation techniques such as precision technology and the introduction of on-demand delivery of irrigation supplies might help in

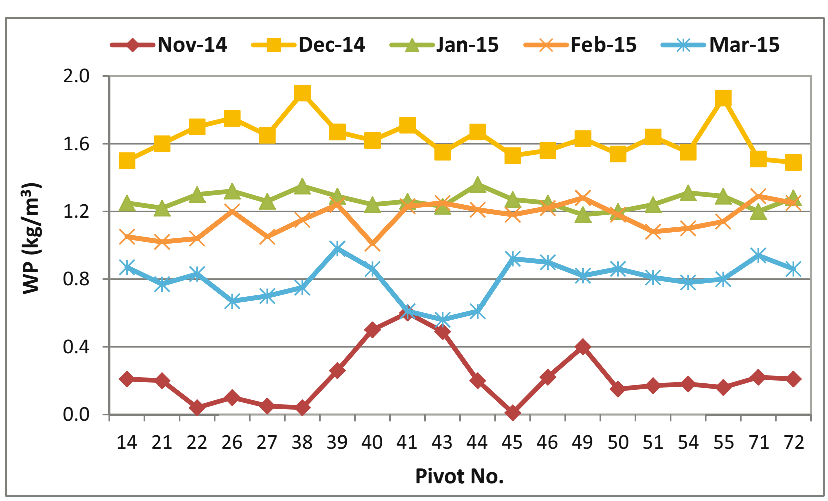

Figure 9: Daily estimated WP during the winter wheat cycle.

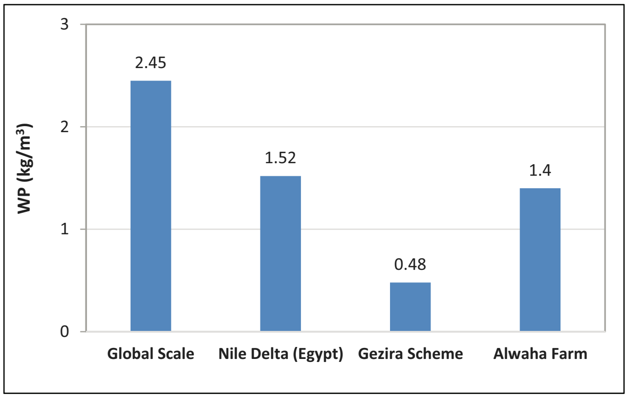

Figure 10: The WP in Alwaha Farm in comparison to the Global Scale [40], Nile Delta [41], and Gezira Scheme [42].

increasing the water use efficiency. However, agronomic practices were the best for achieving higher WP than water management and soil and land management interventions [43].

3.3 Validation of SEBAL model outcome

The FAO P-M was used widely as a standard method to validate the SEBAL model outputs [44,45]. Compared with FAO-PM values, the simulation errors of the SEBAL model were within acceptable limits. The MRE ranged from 2.1 to 11.0% during December 2014–March 2015 (Figure 11a). A significantly high level of agreement was observed between the two methods throughout the growing season of the winter wheat, with an RMSE of 0.35 mm day-1 and NRMSE of 10.4% (Figure 11b). Also, the CV values showed high accuracy in estimating the ETa for the winter wheat compared to the FAO P-M method (Figure 11c). Nevertheless, the actual mean applied irrigation in the farm was slightly lower than that calculated and predicted by the FAO P-M and SEBAL model, respectively (Figure 11d).

The average values of the MRE and the CV were high during March mainly due to the variations between the pivots in the grain growth stage, as some of them were almost in the harvesting stage and the others required several days to reach the maturity stage. Also, the kc of winter wheat can vary during the growing season, depending on their growth stage [46].

Based on these validated parameters, SEBAL could accurately predict winter wheat's field water status and crop growth process. In addition, it incorporates minimum inputs of routine weather data for the ET0 calculation compared to the FAO P-M method, which applied more detailed climate data for this purpose.

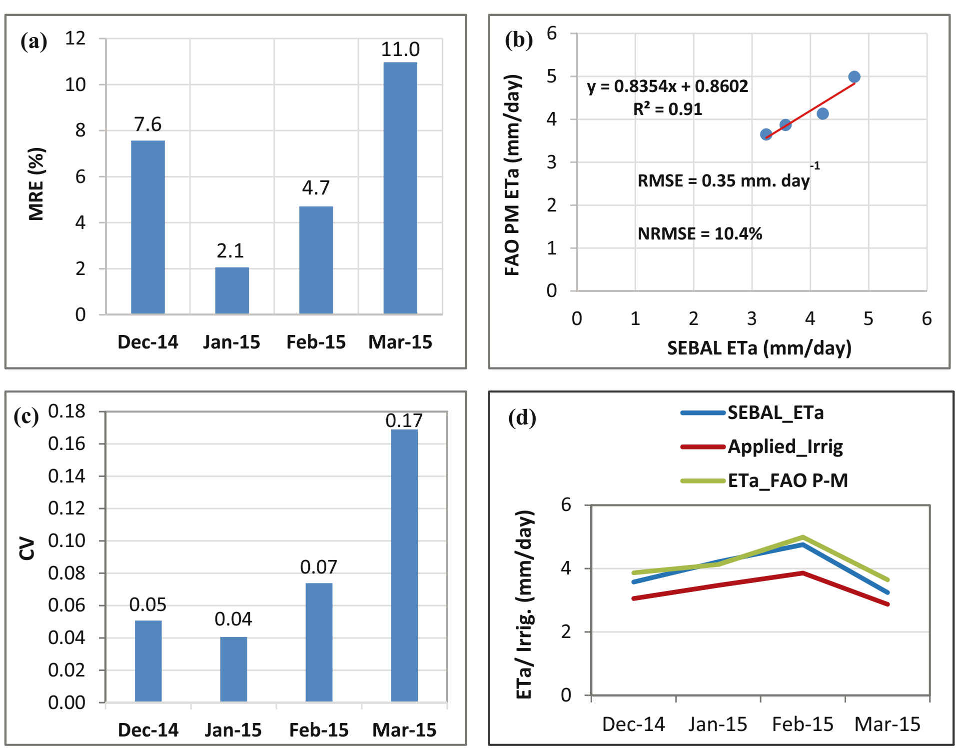

Figure 11: The validation indices between the FAO P-M and SEBAL model: (a) MRE, (b) RMSE and NRMSE, (c) CV, and (d) Water application trends.

The daily agricultural practices at the farm scale, like fertilizers application, drainage, and moisture management, might result in a slight difference between the actual water applied in the field estimated by FAO P-M and SEBAL model.

4 Conclusion

This study demonstrates the power of RS data and biophysical modelling for quantifying the ETa and WP process for the winter wheat in Sudan's semi-arid central clay plain. The estimated seasonal ETa of the winter wheat was 400–600 mm. However, the CWP ranged from 1.2 to 1.5 kg/m^3 during the winter wheat cycle.

The current calculated ETa data agreed well with the FAO P-M standard method. Furthermore, the estimated WP was most likely in good agreement compared to the Nile Delta in Egypt. Nevertheless, it varied significantly compared to the Global Scale and Gezira Scheme (Sudan) data.

The RS input data such as surface albedo, LAI, NDVI, surface temperature (T_s), and DEM make it a highly reliable technique for obtaining the ETa and other crop indicators.

The applied methodology allowed an understanding of the spatial variability of ETa and CWP. Therefore, the Landsat-8 data and SEBAL model have a high potential to estimate the ETa and CWP of the winter wheat's different stages of growth and development. This also helps to understand the need for crop water, improve water use efficiency at the field scale, and estimate the water balance over large agricultural areas. Also, the study shows that agricultural investment by the private sector can play an essential role in sustaining production, food security, and community development.

Acknowledgments: The authors would like to thank the Hydraulics Research Center in Sudan (HRC-Sudan) for providing part of data used in this study.

Funding information: This work was supported by the Deanship of Scientific Research, King Faisal University, Saudi Arabia [NA000219].

Author contributions: Conceptualisation, methodology, software and formal analysis, and writing – original draft preparation, K.G.B. (Turk); writing – review, editing, and supervision, M.A. (Alsanad). All authors have read and agreed to the published version of the manuscript.

Conflict of interest: The authors state no conflict of interest.

Data availability statement: 8 Landsat-8 satellite imageries are available at the United States Geological Survey (USGS) repository, https://earthexplorer.usgs.gov/. Other data sets generated during and/or analysed during the current study are available from the corresponding author upon reasonable request.

References

[1] Yeşilköy S, Şaylan L. Assessment and modelling of crop yield and water footprint of winter wheat by aquacrop. Ital J Agrometeorol. 2020;3:3–14. doi: 10.13128/ijam-859.

[2] Sheta MH, Fayed MH. Productivity and water use efficiency of summer squash crop under two methods of irrigation water application. Egypt J Soil Sci. 2021;61(1):1–11. doi: 10.21608/EJSS.2020.48343.1404.

[3] Kijne J, Barron J, Hoff H, Rockström J, Karlberg L, Gowing J, et al. Opportunities to increase water productivity in agriculture with special reference to Africa and South Asia: A report prepared by Stockholm Environment Institute, for the Swedish Ministry of Environment presentation at CSD 16. New York; 2009.

[4] Molden D, Sakthivadivel R. Water accounting to assess use and productivity of water. Int J Water Resourc Dev. 1999;15:55–71. doi: 10.1080/07900629948934.

[5] Paul M, Rajib A, Negahban-Azar M, Shirmohammadi A, Srivastava P. Improved agricultural water management in data-scarce semi-arid watersheds: Value of integrating remotely sensed leaf area index in hydrological modeling. Sci Total Environ. 2021;791:148177. doi: 10.1016/j.scitotenv.2021.148177.

[6] Calera A, Campos I, Osann A, D'Urso G, Menenti M. Remote sensing for crop water management: from ET modelling to Services for the end Users. Sensors. 2017;17:1104. doi: 10.3390/s17051104.

[7] Knipper KR, Kustas WP, Anderson MC, Nieto H, Alfieri JG, Prueger JH, et al. Using high-spatiotemporal thermal satellite ET retrievals to monitor water use over California vineyards of different climate, vine variety and trellis design. Agric Water Manag. 2020;241:106361. doi: 10.1016/j.agwat.2020.106361.

[8] Usman M, Liedl R, Shahid MA. Managing irrigation water by yield and water productivity assessment of a rice-wheat system using remote sensing. J Irrig Drain Eng. 2014;140(7):04014022. doi: 10.1061/(ASCE)IR.1943-4774.0000732.

[9] Du J, Song K, Wang Z. Estimation of water consumption and productivity for rice through integrating remote sensing and census data in the Songnen Plain, China. Paddy Water Environ. 2015;13:91–9. doi: 10.1007/s10333-013-0411-1.

[10] José JV, de Oliveira NPR, da Silva TJD, Bonfim-Silva EM, Costa JD, Fenner W, et al. Quantification of cotton water consumption by remote sensing. Geocarto Int. 2020;35(16):1800–13. doi: 10.1080/10106049.2019.1583777.

[11] Waqas MM, Waseem M, Ali S, Leta MK, Noor Shah A, Awan UK, et al. Evaluating the spatio-temporal distribution of irrigation water components for water resources management using geo-informatics approach. Sustainability. 2021;13:8607. doi: 10.3390/su13158607.

[12] Li H, Zheng L, Lei Y, Li C, Liu Z, Zhang S. Estimation of water consumption and crop water productivity of winter wheat in North

China Plain using remote sensing technology. Agric Water Manag. 2008;95:1271–8. doi: 10.1016/j.agwat.2008.05.003.

[13] Usman M, Mahmood T, Conrad C, Bodla BH. Remote sensing and modelling based framework for valuing irrigation system efficiency and steering indicators of consumptive water use in an irrigated region. Sustainability. 2020;12:9535. doi: 10.3390/su12229535. 2020.

[14] Awan U, Tischbein B, Conrad C. Remote sensing and hydrological measurements for irrigation performance assessments in a water user association in the lower Amu Darya River Basin. Water Resour Manag. 2011;25:2467–85. doi: 10.1007/s11269-011-9821-2.

[15] Allam M, Mhawej M, Meng Q, Faourc G, Abunnasr Y, Fadel A, et al. Monthly 10-m evapotranspiration rates retrieved by SEBALI with Sentinel-2 and MODIS LST data. Agric Water Manag. 2021;243:106432. doi: 10.1016/j.agwat.2020.106432.

[16] USDA. United States Department of Agriculture; 2021. https://www.indexmundi.com/agriculture/? country = sd&commodity = wheat&graph = production.

[17] FAOSTAT. The Food and Agriculture Organization Corporate Statistical Database; 2021. https://www.fao.faostat/en/#data/QCL.

[18] Rebelo LM, Johnston R, Karimi P, McCornick PG. Determining the dynamics of agricultural water use: cases from Asia and Africa. J Contemp Water Res Educ. 2014;153:79–90. doi: 10.1111/j.1936-704X.2014.03182.x.

[19] Bastiaanssen WGM, Karimi P, Rebelo LM, Duan Z, Senay G, Muttuwatte L, et al. Earth observation based assessment of the water production and water consumption of Nile Basin agro-ecosystems. Remote Sens. 2014;6:10306–34. doi: 10.3390/rs61110306.

[20] Ahmed MAM. Introducing new technologies on the vertisols of Eastern Sudan: A dynamic programming approach. PhD Thesis. USA: Purdue University; 1994.

[21] Malbéteau Y, Merlin O, Gascoin S, Gastellu JP, Mattar C. Correcting land surface temperature data for elevation and illumination effects in mountainous areas: a case study using ASTER data over a steep-sided valley in Morocco. Remote Sens Environ. 2017;189:25–39. doi: 10.1016/j.rse.2016.11.010.

[22] USGS. Department of the Interior United State Geological Survey (USGS). Landsat 8 (L8) Data Users Handbook. LSDS-1574 Version 5.0; 2019 (Accessed: 2020-12-24). https://www.usgs.gov/media/files/landsat-8-data-users-handbook.

[23] GLDAS. Global Land Data Assimilation System; 2015. https://ldas.gsfc.nasa.gov/gldas.

[24] Bastiaanssen WGM, Menenti M, Feddes RA, Holtslag AAM. Remote sensing surface energy balance algorithm for land (SEBAL): 1. Formulation. J Hydrol. 1998;212–213(1–4):198–212. doi: 10.1016/S0022-1694(98)00253-4.

[25] Bastiaanssen WGM, Noordman EJM, Pelgrum H, Davids G, Allen RG. SEBAL for spatially distributed ET under actual management and growing conditions. J Irrig Drain Eng. 2005;131(1):85–93. doi: 10.1061/(ASCE)0733-9437##2005.

[26] Allen RG, Burnett B, Kramber W, Huntington J, Kjaersgaard J, Kilic A, et al. Automated calibration of the metriclandsat evaporation process. J Am Water Resour Assoc. 2013;49(3):563–76. doi: 10.1111/jawr.12056.

[27] Allen RG, Trezza R, Tasumi M. Analytical integrated functions for daily solar radiation on slopes. Agric For Meteorol. 2006;139:55–73. doi: 10.1016/j.agrformet.2006.05.012.

[28] Bastiaanssen WGM, Molden DJ, Makin IW. Remote sensing for irrigated agriculture: examples from research and possible applications. Agric Water Manag. 2000;46:137–55. doi: 10.1016/S0378-3774(00)00080-9.

[29] Mohajane M, Essahlaoui A, Fatiha O, El Hafyani M, El Hmaidi A, El Ouali A, et al. Land use/land cover (LULC) using Landsat data series (MSS, TM, ETM + and OLI) in Azrou Forest, in the central middle Atlas of Morocco. Environments. 2018;5(12):131. doi: 10.3390/environments5120131.

[30] Allen RG, Trezza R, Tasumi M, Kjaersgaard J. Metric: mapping evapotranspiration at high resolution using internalized calibration. Applications Manual for Landsat Satellite Imagery, Version 2.0.8. Kimberly, Idaho, United States: University of Idaho; 2012.

[31] Allen RG, Tasumi M, Trezza R. Satellite-based energy balance for mapping evapotranspiration with internalized calibration (METRIC) – model. American Society of Civil Engineers. J Irrig Drain Eng. 2007;133:380–94. doi: 10.1061/(ASCE)0733-9437.

[32] Allen RG, Pereira LA, Raes D, Smith M. Crop evapotranspiration. FAO Irrigation and Drainage Paper 56. Rome, Italy; 1998.

[33] Wang X, Li L, Ding Y, Xu J, Wang Y, Zhu Y, et al. Adaptation of winter wheat varieties and irrigation patterns under future climate change conditions in Northern China. Agric Water Manag. 2021;243:106409. doi: 10.1016/j.agwat.2020.106409.

[34] FAO. Irrigation and Drainage Paper No. 66, Crop yield response to water. Rome, Italy: Food and Agriculture Organization of the United Nations; 2012.

[35] Al Zayed IS, Elagib NA, Ribbe L, Heinrich J. Spatio-temporal performance of large-scale Gezira Irrigation Scheme, Sudan. Agric Syst. 2015;133:31–142. doi: 10.1016/j.agsy.2014.10.009.

[36] Farming FAO. systems report synthesis of the country reports at the level of the Nile Basin. Rome: Food and Agriculture Organization of the United Nations; 2011. http://www.fao.nr/water/faonile/.

[37] Adeeb AM. Water productivity of food crops in Gezira Scheme, Sudan. In: International Conference on Environmentally Sound Technology in Water Resources Management. Gaborone, Botswana: IASTED-Canada; 11–13 September, 2006. p. 502–802.

[38] Turral H, Burke J, Faures J-M. Climate change, water and food security. FAO Water Reports. Vol. 36. Rome, Italy: FAO; 2011.

[39] Descheemaeker K, Bunting SW, Bindraban P, Muthuri C, Molden D, Beveridge M, et al. Increasing water productivity in agriculture. In: Boelee E, editor. Managing Water and Agroecosystems for Food Security. Wallingford UK: CABI; 2013. p. 104–23.

[40] Bastiaanssen WGM, Steduto P. The water productivity score (WPS) at global and regional level: Methodology and first results from remote sensing measurements of wheat, rice and maize. Sci Total Environ. 2017;575:595–611. doi: 10.1016/j.scitotenv.2016.09.032.

[41] Zwart SJ, Bastiaanssen WGM. SEBAL for detecting spatial variation of water productivity and scope for improvement in eight irrigated wheat systems. Agric Water Manag. 2007;89(3):287–96. doi: 10.1016/j.agwat.2007.02.002.

[42] Ahmed BM, Tanakamaru H, Tada A. Application of remote sensing for estimating crop water requirements, yield and water productivity of wheat in the Gezira Scheme. Int J Remote Sens. 2010;31(16):4281–94. doi: 10.1080/01431160903246733.

[43] Van Opstal J, Droogers P, Kaune A, Steduto P, Perry C. Guidance on realizing real water savings with crop water productivity interventions. FAO Water Reports. Vol. 46. Wageningen: FAO and FutureWater; 2021.
[44] Singh RK, Senay G. Comparison of four different energy balance models for estimating evapotranspiration in the Midwestern United States. Water. 2016;8:9.
[45] Kong J, Hu Y, Yang L, Shan Z, Wang Y. Estimation of evapotranspiration for the blown-sand region in the Ordos basin based on the SEBAL model. Int J Remote Sens. 2019;40(5–6):1945–65.
[46] Mazahrih NTH, Al-Zubi Y, Ghnaim H, Lababdeh L, Ghananeem M, Abu-Ahmadeh H. Determination of actual crop evapotranspiration and crop coefficient of date palm trees (Phoenix dactylifera) in the Jordan Valley. Am-Eurasian J Agric Environ Sci. 2012;12(4):434–43.